Delft University of Technology

Unravelling effects of cooperative adaptive cruise control deactivation on traffic flow characteristics at merging bottlenecks

Xiao, Lin; Wang, Meng; Schakel, Wouter; van Arem, Bart

Important note
To cite this publication, please use the final published version (if applicable).
Please check the document version above.

Unravelling effects of cooperative adaptive cruise control deactivation on traffic flow characteristics at merging bottlenecks

Lin Xiao, Meng Wang[*], Wouter Schakel, Bart van Arem

Department of Transport and Planning, Faculty of Civil Engineering and Geosciences, Delft University of Technology, Stevinweg 1, 2628 CN Delft, the Netherlands

A B S T R A C T

Cooperative Adaptive Cruise Control (CACC) systems have the potential to increase roadway capacity and mitigate traffic congestion thanks to the short following distance enabled by inter-vehicle communication. However, due to limitations in acceleration and deceleration capabilities of CACC systems, deactivation and switch to ACC or human-driven mode will take place when conditions are outside the operational design domain. Given the lack of elaborate models on this interaction, existing CACC traffic flow models have not yet been able to reproduce realistic CACC vehicle behaviour and pay little attention to the influence of system deactivation on traffic flow at bottlenecks. This study aims to gain insights into the influence of CACC on highway operations at merging bottlenecks by using a realistic CACC model that captures driver-system interactions and string length limits. We conduct systematic traffic simulations for various CACC market penetration rates (MPR) to derive free-flow capacity and queue discharge rate of the merging section and compare these to the capacity of a homogeneous pipeline section. The results show that an increased CACC MPR can indeed increase the roadway capacity. However, the resulting capacity in the merging bottleneck is much lower than the pipeline capacity and capacity drop persists in bottleneck scenarios at all CACC MPR levels. It is also found that CACC increases flow heterogeneity due to the switch among different operation modes. A microscopic investigation of the CACC operational mode and trajectories reveals a close relation between CACC deactivation, traffic congestion and flow heterogeneity.

1. Introduction

Connected and automated vehicles (CAVs) have received considerable attention in recent years, since they are seen as a promising solution to mitigate traffic congestion, a source of enormous loss to the economy and society. One concept entails CAVs traveling in very close distance to substantially increase roadway capacity (Ioannou, 1997). To realize that, Cooperative Adaptive Cruise Control (CACC) is often employed, which enables CAVs to maintain a constant time gap with the predecessor automatically. Thanks to the use of Vehicle-to-Vehicle (V2V) communication, CACC vehicles are able to anticipate traffic further downstream and respond faster and earlier so that disturbances can be damped out even when a small time gap is used (Shladover et al., 2015).

Many studies have shown that introducing CACC vehicles in traffic changes the characteristics of traffic flow, such as roadway capacity (VanderWerf et al., 2002, van Arem et al., 2006, Shladover et al., 2012, Arnaout and Arnaout, 2014, Zhao and Sun, 2013)

and flow stability (Schakel et al., 2010, Calvert et al., 2011, Talebpour and Mahmassani, 2016). In particular, roadway capacity attracts the most attention since it presents the great potential of CACC in mitigating traffic congestion. In this study, our scope is limited to the traffic flow characteristics in the presence of CACC vehicles with a focus on roadway capacity.

Existing studies on roadway capacity involving CACC are often carried out via an analytical approach or traffic simulations. Using an analytical approach, roadway capacity is inversely related to the averaged time headway. The individual time headway is determined by the inter-vehicle spacing, vehicle length, and travelling speed. The averaged time headway also depends on the proportions of each vehicle type. In this regard, the CAV spacing control and the mixture of vehicle classes are the determining factors to the capacity in analytical studies. For the spacing control, it is found that the constant time gap control is a more attractive option than the constant spacing control regarding string stability (Swaroop et al., 1994), so it is widely accepted in commercial CACC systems and assumed in most of the capacity studies. The chosen time gap for CACC should consider vehicle braking capability as a constraint (Kanaris et al., 1997, Michael et al., 1998) and the capacity estimation should consider the headway/time gap stochasticity (Ghiasi et al., 2017). Regarding vehicle classes, it is found that the roadway capacity is sensitive to the ratios of vehicle classes in mixed traffic, due to various time gap settings for each vehicle class. Introducing 10% new vehicles with large desired time gap could lead to a capacity reduction of 15% at a highway segment and of 40% at a merging section (Michael et al., 1998, Hall and Li, 1999). Besides that, Chen et al. (2017) shows that roadway capacity increases with the CAV penetration rate and platoon size, and a mixed-used lane for both CAVs and conventional vehicles can realize higher capacity than a strict segregation between these two types of vehicles. In addition, Tientrakool et al. (2011) examined the capacity change in terms of vehicle connectivity. The result shows that using radar sensor along with V2V communication provides a larger capacity increase than using sensors alone, which suggests the superiority of CACC system compared with the ACC system.

Analytical approaches are based on macroscopic traffic flow models and allow us to identify and explain the impact of a limited number of factors introduced by CACC vehicles. However, analytical approaches typically model the traffic flow in equilibrium states, and do not capture well the nonlinear phenomena in traffic flow such as flow instability and capacity drop. In this regard, the capacity estimated via analytical approaches is often higher than the maximum throughput in observation.

In order to assess the achievable roadway capacity with CACC vehicles, a number of studies evaluate the impacts through microscopic traffic simulations. How the car-following behaviour of CACC vehicles is modelled determines to a large extent the resulting capacity. There are three types of car-following models for C-ACC vehicles typically used in existing simulations. The first group of studies uses a car-following model for manually driven vehicles with different time gap settings for automated vehicles. The intelligent driver model (IDM) was chosen for simulating adaptive cruise control vehicles in Kesting et al. (2008) and connected vehicles in Guériau et al. (2016), and the optimal velocity model (OVM) was selected for connected cruise control vehicles in Ge and Orosz (2017). Although this method is easy to be implemented, the human driver models are not able to produce realistic behaviour of automated vehicles since they neglect the multiple sub-controllers and various driving modes in an automated control system and their resulting complicated vehicle behaviour. The second group of studies uses the desired accelerations of the CACC control algorithms, either the linear constant time gap control or more sophisticated nonlinear algorithms with safety constraints to avoid rear-end collisions (Wang et al., 2016b), as actual vehicle accelerations (VanderWerf et al., 2002, van Arem et al., 2006, Shladover et al., 2012, Zhao and Sun, 2013, Schakel et al., 2010, Talebpour and Mahmassani, 2016, Tientrakool et al., 2011, Makridis et al., 2017). However, the outputs of CACC controllers do not represent closed-loop CACC vehicle behaviour, since the mechanical driveline dynamics and rolling and aerodynamic resistance are not taken into account. The third group of studies uses an empirical CACC car-following model that is derived from field test experiments, relating the realized vehicle accelerations/speeds with relative speed and distance to predecessors. An empirical model was established in Milanes and Shladover (2014) and calibrated using vehicle trajectory from a field test of four CACC vehicles on public roads. This model is able to produce realistic CACC vehicle response within the high-speed range in which the field test data has been collected, but is not collision-free in a low-speed range. To apply it in a microscopic simulation, a previous study (Xiao et al., 2017) extended the empirical model into a full-speed-range CACC car-following model. It includes a speed-varying spacing margin for low-speed range and a driver-automation interaction module in which a driver can deactivate the CACC system and take over vehicle control. This model offers a realistic speed and acceleration profile for CACC vehicles in several typical scenarios with explicitly captured driver-automation interaction.

In addition to the car-following model, the network topology and CACC market penetration rate (MPR) are also critical factors for the capacity estimation in simulation-based studies. In the simulations of a single-lane highway with an on-ramp and off-ramp, the maximum lane throughput increases with a decrease of desired time gap (VanderWerf et al., 2001) and exhibits a quadratic increase with CACC MPR (VanderWerf et al., 2002). Based on a hypothetical single lane highway with an on-ramp, another study investigated the impacts of CACC vehicles on string stability and throughput and confirmed that CACC vehicles increase throughput (Talebpour and Mahmassani, 2016). However, the results of single-lane simulations cannot represent the capacity of multi-lane highways because the influences of lane changes are not taken into account. In this regard, other studies examined the CACC impacts in a simulated multi-lane highway. A lane drop scenario from a 4-lane section to a 3-lane section is simulated in van Arem et al. (2006). With the analysis of traffic performance with increasing CACC vehicles, this study showed that using CACC vehicles has potential positive impacts on the roadway capacity near a lane drop but a low CACC penetration below 40% does not show significant effects. Liu et al. (2018b) investigated the multi-lane throughput at various CACC MPRs in a simple merging segment. A quadratic relationship is found between the merging throughput and CACC MPR, suggesting that the traffic performance of an on-ramp merging area can also be improved by CACC vehicles. For a weaving segment, Tilg et al. (2018) evaluated the effects of the reduced reaction time by vehicle automation on flow operation via a hybrid multi-class model. The results show a non-linear increase of the capacity in the weaving segment with an increasing vehicle MPR. Hartmann et al. (2017) and Makridis et al. (2017) simulated CACC vehicles in German highway network and the ring road of Antwerp respectively for different market penetration rates. Both simulation results

confirmed the potential of CACC vehicles to increase roadway capacity in a real traffic network. Additionally, Makridis et al. (2017) pointed out that the capacity increase in a basic multi-lane segment and merging segment are only up to around 45% and 40% in the 100% CACC case. Zhao and Sun (2013) and Arnaout and Bowling (2011) investigated the impacts of CACC MPR on roadway capacity/throughput in a multi-lane highway, but they assumed no lane change is performed during the simulation. The pipeline capacity of a two-lane highway is around 3000 veh/h/lane with 100% CACC (Zhao and Sun, 2013), while the maximum throughput at an on-ramp merging section is proportional to the CACC MPR and vehicle arrival rate, at around 1952 veh/h/lane with an 8000 veh/h arriving rate in 100% CACC vehicles case (Arnaout and Bowling, 2011).

Apart from car-following models and simulation networks, roadway capacity is highly related to the assumptions made for vehicle time gaps in simulations. It is noticed that most abovementioned studies (VanderWerf et al., 2002, van Arem et al., 2006, Arnaout and Bowling, 2011, Zhao and Sun, 2013) use a 0.5 s time gap for CACC vehicles. It is a much smaller value compared to the time gap of manual driving, and therefore it contributes significantly to the roadway capacity increase. However, in real traffic, drivers choose different time gaps settings of automated vehicles, and most of them are larger than 0.5 s (Nowakowski et al., 2011). Using a realistic distribution of time gap setting from a field test, the lane capacity based on a single-lane simulation is reduced to 3970 veh/h/lane in 100% CACC case (Nowakowski et al., 2011), compared to 4550 veh/h/lane in the earlier studies (VanderWerf et al., 2002). This shows that CACC time gap setting plays a determinate role in the resulting capacity in simulations and a higher desired time gap leads to a lower attainable capacity increase. The CACC MPR straightforwardly determines the weight of CACC time gaps among the overall traffic and thus the capacity increase is highly sensitive to both CACC MPR and time gaps. A similar conclusion has been drawn by Kesting et al. (2010) in impact analysis of ACC vehicles.

In summary, the estimated roadway capacity with CACC vehicles varies largely in different simulation studies. Difference can be explained by the differences in the car-following and lane change models, desired time gap settings, simulation networks, and CACC MPRs. Among these studies, assumptions without empirical evidence were widely made, such as (1) using vehicle control algorithm as car-following response; (2) no authority transitions involved with CACC operation; (3) overestimated CACC performance in maintaining desired time gaps less than 0.5 s and (4) infinite CACC string length. To this end, the actual impacts of CACC vehicles on road flows remain uncertain. This study keeps the simulation realism as much as possible in order to provide a reliable evaluation of the CACC vehicle impacts on traffic flow characteristics. The simulation realism includes using an empirically underpinned car-following model, realistic time gap settings, plausible lane change behaviour induced by CACC authority transitions, and a practical constraint in CACC string length. Moreover, another contribution of this study is to show to what extent CACC vehicles can increase the roadway capacity at different MPRs, given the realistic behavioural model and time gaps. In particular, we focus on both the free-flow capacity and the queue discharge rate, which is paid less attention to by most of the existing CACC studies. Thus, the two-capacity phenomenon (Banks, 1991) and capacity drop can be discussed in this paper. The setting allows the discovery of both equilibrium and dynamical characteristics of congested flow in relation to different CACC MPRs.

This paper builds on the multi-regime car-following model for CACC systems proposed in our previous study (Xiao et al., 2017). The model extends the empirical model (Milanes and Shladover, 2014) to full speed range, generates constant time gap behaviour at equilibrium conditions, and captures two types of authority transitions (system-initiated and driver-initiated). In this study, we further improve this model into a multi-lane scenario by integrating the car-following model into a Lane Change Model with Relaxation and Synchronization (LMRS) (Schakel et al., 2012). The integrated simulation model is applied to a merging bottleneck where systematic simulation experiments are conducted. The experiment provides an evaluation of the CACC vehicle impacts on traffic flow characteristics, with a focus on flow-density relations, capacity and capacity drop. The evaluation is conducted for different levels of CACC market penetration rates, to show the changes by increased numbers of CACC vehicles in the near and long-term future.

In Section 2 we introduce the CACC behaviour model for multi-lane traffic, including the car-following model, lane change model, the driver-system interaction and string operation. Section 3 presents the experimental design for the impact analysis of CACC vehicle market penetration rates for a pipeline scenario and a merging bottleneck scenario. The simulation results are shown in Section 4, followed by a discussion in Section 5. Conclusions and future work are provided in Section 6.

2. CACC behaviour model for multi-lane traffic

In this section, we first look into the car-following models of CACC vehicles and conventional vehicles respectively and then the lane change model for multi-lane traffic. After that, we present the assumptions of CACC system deactivation and reactivation, as well as the switching conditions for different vehicle modes and the vehicle behaviour in transitions. Next, we elaborate on CACC string operation including the string definition, properties and manoeuvres. Finally, we describe the model implementation in a microscopic simulation framework.

2.1. Car-following model

2.1.1. Control framework

A multi-regime car-following model of CACC vehicles has been previously elaborated in Xiao et al. (2017), where the longitudinal vehicle response is modelled with two parallel control loops. Both the human driver control loop and the (C)ACC control loop are based on a three-stage (perception – decision-making – actuation) control structure and it represents the sequential procedure for the underlying physics of vehicle longitudinal behaviour in discrete time steps (Milanés et al., 2014). Fig. 1 illustrates the dual loop control, where v_i, x_i and a_i refer to the speed, position and realized acceleration of vehicle i. At each time step, the speed and position
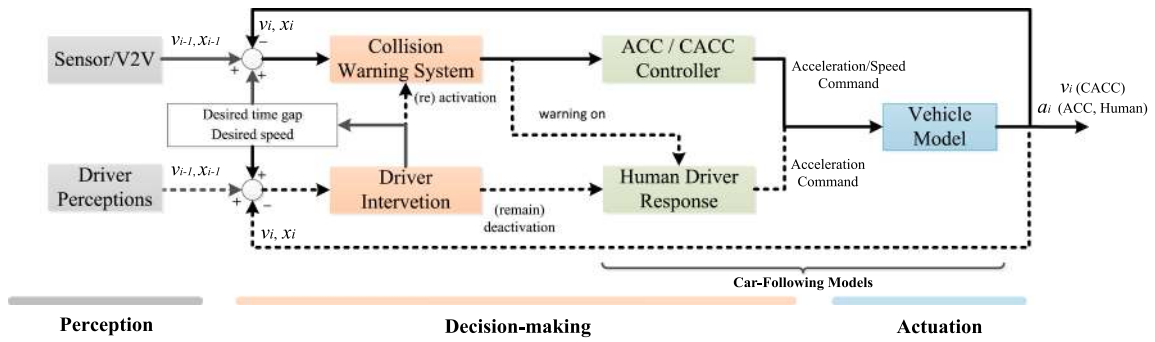
Fig. 1. Conceptual longitudinal model for CACC vehicles in simulations.

of preceding vehicle $i-1$ and subject vehicle i at a previous time step, as well as the desired time gap and the cruising speed, are used either by the CACC algorithm or by the human driver to determine the acceleration or speed command to the vehicle. The lower-level vehicle actuators will execute the acceleration/speed command and generate the (realized) acceleration/speed response. Note that the realized speed and acceleration may differ from the commanded values due to the driveline dynamics and resistance of rolling and aerodynamic drag mentioned in the Introduction section. Our car-following model captures the relation between the realized acceleration/speed and the vehicle position and speeds rather than detailing the ACC/CACC algorithms and lower-level vehicle dynamics.

2.1.2. Model specification

With the dual loop control, the CACC vehicles have three possible vehicle operating systems: manual driving, ACC operation and CACC operation. The ACC and CACC operation include sub-controllers for three different control objectives (Milanés and Shladover, 2015):

- a cruising controller to maintain a user-set desired speed if a preceding vehicle is absent;
- a gap-regulating controller to maintain a constant time gap with its predecessor in car-following situations;
- a gap-closing controller performing a transition from the cruising controller to the gap regulation controller when an ACC/CACC vehicle approaches its leader from long distance.

The vehicle state using a particular sub-controller is referred as the vehicle mode in our study. Each mode in these operations has its own car-following model, of which the mathematical specifications and the switching logics are described as following.

2.1.3. Cruising mode

The control objective of the cruising mode is to maintain the user-desired speed when the preceding vehicle is absent or far away and the vehicle acceleration is modeled as:

$$a_{i,k} = k_0 \cdot (v_{set} - v_{i,k-1}) \tag{1}$$

where the control gain k_0 is a parameter to determine the rate of speed error for acceleration and v_{set} is the driver's desired speed. The value of k_0 is assumed as $0.4\,\mathrm{s}^{-1}$ (Xiao et al., 2017).

2.1.4. Gap-regulating mode

In the gap-regulating mode, the car-following response of ACC vehicles is described by

$$a_{i,k} = k_1 \cdot e_{i,k} + k_2 \cdot (v_{i-1,k-1} - v_{i,k-1}) \tag{2}$$

where $e_{i,k}$ is the gap error of vehicle i at time step k. It shows that the vehicle acceleration depends on a gap error and a speed difference with the preceding vehicle, where their feedback gains k_1 and k_2 are $0.23\,\mathrm{s}^{-2}$ and $0.07\,\mathrm{s}^{-1}$ respectively (Milanes and Shladover, 2014).

For vehicles under CACC control, vehicle's speed is calculated by the speed in previous time step $v_{i,k-1}$, the gap error $e_{i,k-1}$ in the previous time step and its derivative, according to

$$v_{i,k} = v_{i,k-1} + k_p \cdot e_{i,k-1} + k_d \cdot \frac{(e_{i,k-1} - e_{i,k-2})}{\Delta t} \tag{3}$$

where k_p and k_d are $0.45\,\mathrm{s}^{-1}$ (Milanes and Shladover, 2014) and 0.0125 (Liu et al., 2018a)

The gap error in Eqs. (2) and (3) is determined by Eq. (4), where the inter-vehicle spacing $(x_{i-1,k-1} - x_{i,k-1})$, desired time gap t_{des}, subject vehicle speed $v_{i,k-1}$, vehicle length L and spacing margin d_0 are included.

$$e_{i,k} = x_{i-1,k-1} - x_{i,k-1} - L - t_{des} \cdot v_{i,k-1} - d_0 \tag{4}$$

ACC and CACC car-following models require a different spacing margin, since their collision risks at low speeds are different. Preliminary tests showed that the ACC model should have a 2-meter additional clearance at a speed under 10 m/s while the CACC model requires only 1 m of spacing margin at speeds below 2 m/s. The dynamic spacing margins for ACC and CACC models are therefore formulated as a function of vehicle speed, as shown in Eqs. (5) and (6) respectively.

$$d_0 = \begin{cases} 0 & v \geqslant 15\,\text{m/s} \\ \frac{75}{v} - 5 & 10.8 \leqslant v \leqslant 15\,\text{m/s} \\ 2 & v < 10.8\,\text{m/s} \end{cases} \tag{5}$$

$$d_0 = \begin{cases} 0 & v \geqslant 10\,\text{m/s} \\ -0.125v & v < 10\,\text{m/s} \end{cases} \tag{6}$$

2.1.5. Gap-closing mode

Reducing the speed difference and shortening the gap are the control objectives of the gap-closing controller. To achieve a safe approach, we increase the feedback gain on speed error and reduce the feedback gain on gap error. After tuning, k_1 and k_2 are 0.04 s^{-2} and 0.8 s^{-1} in Eq. (2), k_p and k_d are 0.005 s^{-1} and 0.05 in Eq. (3). These approaching models in combination with the driver intervention are able to guarantee collision-free driving when a CACC vehicle approaches a standstill vehicle, either under ACC control or CACC control (Xiao et al., 2017).

Three driving modes fulfil the different purposes of a vehicle moving and the switches among them are responses to the interaction between the subject vehicle and the environment. The cruising mode is operated when there is no leader in front and the vehicle maintains the desired speed. If a leader is found, depending on the distance with the leader, either the gap-regulating or gap-closing mode takes over. If the actual gap to the leader is larger than 1.5 times of the desired gap, the subject vehicle operates at the gap-closing mode, otherwise it operates at gap-regulating mode. The criterion of switching from gap-closing mode to gap-regulating mode is that the gap error is smaller than 0.05 m (Xiao et al., 2017).

Two assumptions are made for the accelerations determined in different driving modes. Firstly, to prevent CACC vehicles exceeding their desired speeds, the free-flow acceleration calculated by the cruising model is taken as the upper bound of the accelerations in gap-regulating and gap-closing models. If the gap-regulating model or gap-closing model generates higher accelerations than the free-flow acceleration, the latter will be used. Secondly, the accelerations from ACC/CACC models are limited to a range from $-4\,\text{m/s}^2$ to $2\,\text{m/s}^2$. This assumption is made according to the internal acceleration limitations posed on production ACC vehicles (Milanes and Shladover, 2014).

2.1.6. Manual driving

The car-following model for human drivers is a modified version of the Intelligent Driver Model (Treiber et al., 2000), referred to as IDM+ (Schakel et al., 2010). The IDM+ provides the desired acceleration as the minimum of the acceleration of driving towards the desired speed and the acceleration towards the desired headway. Compare to the IDM, the IDM+ is able to achieve more reasonable values of capacity.

2.2. Lane change model

The lane change model we implemented for all vehicle types is based on the Lane Change Model with Relaxation and Synchronization (LMRS) in Schakel et al. (2012). In the LMRS, the lane change behaviour is predicted by a decision model that calculates the lane change desire first and determines whether a lane change is needed and which type of lane change should be executed. The lane change desire is the weighted summation of multiple lane change incentives for following the route, gaining speeds and respecting traffic rules such as keep-right directive. The route incentive is a mandatory incentive while the other two incentives are discretionary incentives. The weight for discretionary incentives becomes smaller when the route incentive appears (Schakel et al., 2012). The lane change desire is formulated as:

$$d^{ij} = d_r^{ij} + \theta^{ij} \cdot (d_s^{ij} + d_b^{ij})$$

where d^{ij} is the overall lane change desire from lane i to lane j. d_r^{ij}, d_s^{ij} and d_b^{ij} represent the incentives for the route, speed and a directional bias respectively, and θ^{ij} is a weight factor reflecting the relative importance of discretionary incentives.

The magnitude of the lane change desire results in four different types of lane change behaviour, being No Lane Change (No LC), free lane changes (FLC), synchronized lane changes (SLC) and cooperative lane changes (CLC). Fig. 2 shows the relationships between lane change desire and the resulting lane change behaviour, with behavioural changes in synchronization and gap-creation. The synchronization refers to the speed synchronization between the lane changer and its target leader, and the gap-creation refers to a courtesy provided by the potential follower in the target lane to facilitate the lane change. In SLC, the lane changer aligns its speed with that of the leader in the target lane, but the follower in the target lane does not actively create a gap for the lane changer. As the desire exceeds the CLC criteria, cooperative lane changes (CLC) are expected, in which the lane changing vehicle synchronizes its speed with the potential leader in the target lane and the potential follower in target lane actively creates a gap in front for the lane changer.

The interaction between the lateral and longitudinal vehicle behaviour is modeled by expressing the acceptable gap and
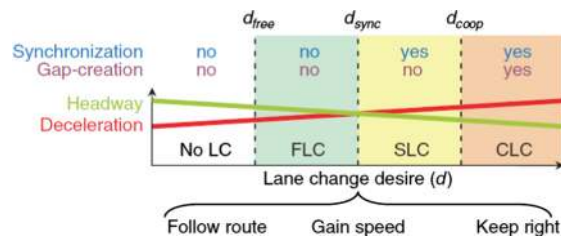
Fig. 2. Four types of lane change behaviour corresponding to the level of lane change desire (Schakel et al., 2012).

acceleration level as functions of the lane change desire. Larger lane change desires lead to smaller acceptable headways and larger decelerations. When the lane change desire is larger than the synchronized lane change threshold, drivers apply the car following model to a leading vehicle in the adjacent lane, resulting in an acceleration for speed synchronization by the subject vehicle or gap creation by the potential follower in the target lane if the desire is even larger and above the cooperation threshold. This acceleration is constrained by a minimum value for comfort and safety. For detailed formulas and specifications of the lane change model and gap acceptance model, we refer to Schakel et al. (2012).

The LMRS was extended and calibrated for situations with U.S. traffic, including the use of dedicated lanes in a previous study (Xiao et al., 2016). The resulting extended LMRS is capable of reproducing traffic flow characteristics in a complex network with interacting bottlenecks and HOV lanes, for a long simulation time period during which traffic demand varies considerably.

For CACC systems, it is the responsibility of drivers to make the lane change decisions and perform lane change control. Thus the same lane change model is used for CACC vehicles. When drivers need to change lane to follower route or perform synchronized and cooperative lane changes, drivers need to dynamically adjust the gap and speed to prepare for lane change. In these conditions, deactivating the CACC is needed to pass the vehicle control from the automated system to the human driver.

2.3. System deactivation and reactivation

Studies of automation-driver interaction suggest that authority transitions of automated vehicles have a large influence on traffic flow and they should be taken into account when the impacts of CACC vehicles are investigated (Pauwelussen and Minderhoud, 2008, Pauwelussen and Feenstra, 2010, Klunder et al., 2009, Viti et al., 2008, Varotto et al., 2015). The authority transition of CACC vehicles includes the deactivation and reactivation of the automation system. CACC might be deactivated for discretionary over-ruling, e.g. speed adaptation before a lane change or due to curtesy yielding behaviour, as well as for mandatory overruling such as reaching the system control boundaries or system failures (Pauwelussen and Minderhoud, 2008, Pauwelussen and Feenstra, 2010, Varotto et al., 2015, Klunder et al., 2009). Once CACC is deactivated, it can be reactivated after a certain time period (Viti et al., 2008). During the inactive period, the human drivers take over control and increase the CACC time gap to a manual driving gap, which has great implications for roadway capacity and flow heterogeneity.

2.3.1. Assumptions

The connection and interaction between the ACC/CACC car-following models and the human driver car-following model take place through the system activation/deactivation module. The system activation/deactivation module specifies the switching logic between these two parallel control loops and defines the vehicle behaviour during the transitional period.

One important assumption in this CACC simulation is that drivers intend to use the CACC system as much as possible. With an activated CACC system, three types of system deactivation could take place according to the drivers' intentions. Table 1 lists the deactivation types with detailed scenarios and the minimum time period of remaining deactivated to avoid frequent deactivation within a short time period. In addition, we assume that the CACC system cannot be (re)activated for vehicles braking over $2\,m/s^2$ or performing a lane-change. Drivers' continuous attention of surrounding environment is assumed for the activation and deactivation of CACC, which is plausible since drivers are kept in the control loop for Level 1 automated driving system according to SAE.

The first type of system deactivation is due to increased risk of rear-end collisions. It includes the system-initiated deactivation and the driver-initiated deactivation (see Fig. 1). For system-initiated deactivation, a collision warning model is employed for identifying the safety-critical situations and if a warning is issued, the CACC system will be deactivated and the model switches to

Table 1
Clarification of CACC system deactivations.

Deactivation types	Scenario	Reactivation after
Type I	Collision warning	5 s
Safety-related	Critical approaching	10 s
Type II	Synchronization for lane change	2 s
Lane-change-related	Create a gap for cooperative lane changes	2 s
Type III	Taking exits, merging, lane drop	Arriving at the target lane
Route-related		

human driver mode. The collision warning is determined by an empirically underpinned indicator based on inverse time-to-collision (Kiefer et al., 2005). For driver-initiated deactivation, the driver actively resumes vehicle control in the high-relative-speed approaching scenario, which implies a high risk of rear-end collisions for ACC/CACC vehicles due to the large deviation from equilibrium conditions that cannot be handled by the linear ACC/CACC controller. We assume that if the subject CACC vehicle is approaching the low-speed leader with a relative speed larger than 15 m/s and the gap is less than 150 m, the driver-initiated deactivation will take place.

The second type of system deactivation is related to lane changes, in particular in demanding lane change scenarios where drivers need to actively adjust the longitudinal speed to prepare a lane change or to yield a gap for another lane changer. The deactivation is considered as driver-initiated and the demanding scenarios are captured in the LMRS with high lane change desire. The lane-change-related deactivation appears in synchronized lane changes (SLC) and cooperative lane changes (CLC). When a CACC vehicle has to synchronize its speed with the target leader in the adjacent lane, the ACC/CACC will be first deactivated and then the vehicle switches to human-driven mode. When a CACC vehicle is involved in a cooperative lane change either as the lane changer who synchronizes its speed with the target leader or as the target follower who slows down to yield a gap for the potential lane changer in the adjacent lane, the human driver resumes vehicle control as well after the system deactivation. There is no difference in deactivation in terms of timing and conditions for ACC and CACC. The ACC/CACC system remains active for free lane change (FLC), during which a vehicle does not have to adjust its speed before or after the lane change.

The third type of system deactivation is related to mandatory lane changes, assuming that when vehicles have to make mandatory lane changes, drivers will resume control to avoid frequent switching between automation and human-driven modes. Mandatory lane change is captured by the route incentive in the LMRS model. Once the route incentive has appeared, as soon as the vehicles start to change lanes, the ACC/CACC system is switched off and it will remain inactive until no more lane changes for the route are required. After the route incentive vanishes, the ACC/CACC system can be re-activated if the activation conditions are met.

2.3.2. Switching and transitions

As Fig. 3 illustrates, the switching path of system activation is different than the path of system deactivation. The CACC is considered as an advanced version of the ACC since it additionally requires a DSRC-equipped leader for system activation. If the leader of a CACC vehicle is not equipped with DSRC, the system degrades to ACC operation. ACC operation is therefore chosen as the default control in the automation system and the activation of CACC operation is only possible via the ACC, instead of a direct activation from manual driving. This corresponds well to driver behavioUr that drivers only choose to activate the automation system, rather than choose the ACC or CACC in particularly. For automation deactivation, both ACC and CACC operations can directly be switched to the manual driving, since human drivers should be able to resume controls from any automation status for any aforementioned reason at current SAE Level 1 automation that the driving automation system only executes parts of the lateral and longitudinal vehicle motion control.

The model assumes a gradual transition from automated control to manual driving, since vehicle motions are constrained by vehicle acceleration capability, safety and driving comfort. One notable difference in the behaviour of a CACC vehicle in different modes is the equilibrium time gap. Hence, switching between modes entails transition from one desired time gap to another. For CACC control, the desired time gaps range from 0.6 s to 1.1 s, which are smaller than the 1.4 s of manual driving. Switching the desired time gap from the CACC system to IDM + instantaneously may cause large decelerations and disturbances to upstream flows,
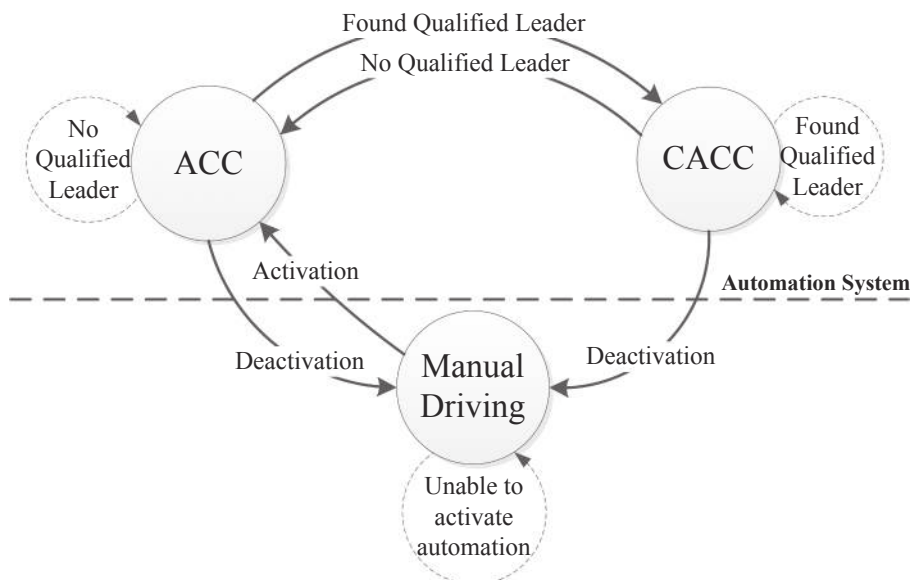

Fig. 3. Switching paths between manual driving, ACC and CACC.

which is disfavoured by drivers and considered unrealistic. We model the transition by gradually changing the time gap of ACC/CACC to that of human drivers under a relaxation process, as suggested in Milanés and Shladover (2015) for a change in desired time in a cut-in scenario. This relaxation process during mode transition produces a smooth acceleration profile for the involved vehicles.

2.4. CACC string operation

A CACC vehicle string is defined as a cluster of CACC vehicles traveling in a lane with short following gaps using V2V communication. The vehicle in the first (front) position of a string is referred to as the string leader and the other vehicles in the string are called string followers. Each follower receives the kinematic information from the string leader and the directly preceding vehicle. This connectivity structure comes from the CACC vehicle string in the field test where the empirical models have been derived, and any non-CACC vehicle traveling between CACC vehicles causes a separation in connectivity. The destinations and desired time gaps of CACC vehicles in a string do not have to be identical (Rajamani et al., 2000).

A CACC vehicle is considered as a CACC string follower when all following three conditions are met: (1) the automation system is activated and the CACC vehicle is in CACC operation; (2) the vehicle is in gap-regulating mode; (3) the vehicle maintains the intra-string gap as the desired time gap instead of the inter-string gap. If one of the conditions is not met, a CACC vehicle is considered as a string leader.

The intra-string and inter-string gap is related to the implementation of string length control. Shladover et al. (2015) suggests that the CACC vehicle string length cannot go to infinity due to V2V communication range limitation, string instability and potential problems it brings at merging/weaving sections. In this regard, we implement a string length limit of 10 vehicles in the simulation to prevent overlong CACC vehicle strings, and a large inter-string gap is defined for the separation between strings. The length limit is assumed based on the maximum vehicle number travelling at highway speed within a V2V communication range of 300 m. Such string operation has been considered in macroscopic modeling (Michael et al., 1998, Hall and Li, 1999, Chen et al., 2017), but is rarely taken into account in microscopic simulations for CACC impact evaluation. The length limit constrains the *string join manoeuvre* that a CACC vehicle or a string of vehicles intend to join an existing string: only when the total string length after the join manoeuvre does not exceed the length limit will the join and intra-string gap be allowed. Otherwise, the leader of the upstream string operates at CACC mode with the inter-string gap to the tail vehicle of the downstream string.

We assume an ad-hoc clustering strategy for CACC strings in our simulation. The formation is conducted by a vehicle or a string joining an existing string. The *join manoeuvre* takes place at the string head or tail when a fast-speed follower/string catches up the leading vehicle/string under the string length limit, and also possible in the middle of a string that a CACC vehicle performs a lane change to the middle position of a string, but this could subject to CACC deactivations and a string separation. The *leave manoeuvre* can take place in any position of the string and consists of three steps. The driver of a leaving vehicle firstly deactivates the CACC operation, and then resumes vehicle control after the transition period in which the gap is gradually increased. When an acceptable gap is found in the target lane, the vehicle performs a lane change and the *leave manoeuvre* is completed. Based on these two manoeuvres, a dynamic CACC string operation can be implemented in the simulation.

2.5. Model implementation

The CACC simulation model was implemented in an open-source microscopic traffic simulation MOTUS for its explicit knowledge of simulated objects and a flexible framework that is easy to be extended for CACC algorithms (Schakel, 2015). Different simulation modules in MOTUS were extended or modified for new vehicle hardware and additional control functionalities. Most of the changes were made to the *Vehicle* module, especially on its secondary On-Board Units (OBU) module for ACC/CACC algorithms and the *Driver* module for new driver behaviour.

The *On-Board Unit* module enables modeling of vehicle connectivity and ACC/CACC electronic control units (ECU). The cyber-physical process of vehicle sensor and V2V communication is not modeled explicitly. Instead, the vehicle information provided by them is realized via accessible data within a certain range and the data is assumed accurate and reliable without any delay or loss. The ACC/CACC algorithm is written in ACC/CACC ECU that is designed depending on the architecture of the controllers in the CACC system. Both of them can override human driver controls when the automation system is activated. Driver behaviour as well as their interaction with the automation systems are implemented in the *Driver* module.

3. Experiment design

To study the impacts of CACC on traffic flow characteristics, we simulate a merging bottleneck where jams often emerge on highways and the capacity drop exists. The simulated network consists of a four-lane highway segment with a single-lane on-ramp. As shown in Fig. 4, the network is 11 km in length and the on-ramp is located at 8 km downstream from the beginning, with an acceleration lane of 250 m. In the first 3 km of the simulated network, the individually generated CACC vehicles will naturally form CACC strings via the *join manoeuvre*. Thus the first 3 km is used as a warm-up section in the simulation.

Three groups of detectors are placed at the locations illustrated as D1, D2, and D3 in Fig. 4 at 8000 m, 8450 m and 10,750 m respectively. D1 is placed at the beginning of the onramp section and aims to determine the traffic states of the merging section. D2 aims to collect the maximum throughput after the merge and therefore it is placed at 200 m downstream from where the onramp section ends. D3 is placed at a further downstream section that is 2500 m away, aiming to collect the queue discharge rate in stable flow conditions according to Yuan et al. (2015). All detectors provide 5-min data for flow and speed.
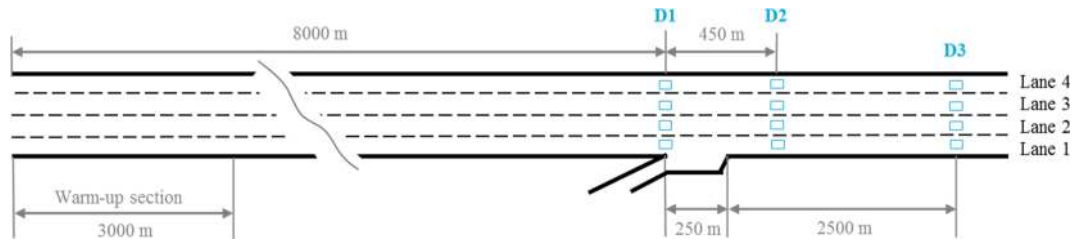
Fig. 4. Road sketch of a simple merging network with detector locations.

To explore the traffic characteristics of mixed CACC vehicles at merging bottlenecks, the CACC MPR is the main control variable. In addition, the on-ramp demand is used as another control variable to simulate different merging disturbances. The CACC MPR increases from 0% to 100% with a 20% increment and applies to all traffic demands, including the mainline and merging traffic. The on-ramp demand is set to 400, 800, 1200 and 1600 veh/h, in order to evoke different levels of merging disturbances. In total, we simulated 24 scenarios, with 5 repetitions of each scenario with different random seeds. The random seed assigns the vehicle class, desired speed and the arriving interval between two vehicles at the simulation generators. The simulation lasts for one hour with a 0.1 s time step and the first 10 min is taken as a warm-up period. In addition, the mainline demand is set to 80% of the capacity of the corresponding CACC MPRs in a pipeline section, assuring that mainline flows are sensitive to the merging disturbances and they could experience the free flow, capacity flow and congested flow at each CACC MPR with the change to the on-ramp demands.

The parameters of the car-following model and simulation settings are listed in Table 2. We assume there is no difference in the vehicle size between the conventional vehicles and CACC vehicles and they both follow the same free-flow speed distribution. The manual driving time gap is assumed as 1.4 s from the calibration outputs of our previous study (Xiao et al., 2016), and the desired time gaps for CACC are selected from drivers' realistic choices in the field test (Shladover et al., 2012). When CACC vehicles are operated under ACC, the desired time gap is set to 1.1 s.

We use the section-based harmonic speed as the traffic state indicator to distinguish the free flows and congested flows from merging bottlenecks. When the speed at D1 is above 80 km/h, traffic is considered to be in free flow and the flow count at D2 is recorded. When the speed is below 80 km/h, traffic is considered congested and the flow count at D3 is stored. The merging capacity is the maximum recorded flow counts at D2, while the queue discharge rate is the averaged throughput stored at D3 for a stable value without influenced by a stop-and-go wave.

In order to estimate the pipeline capacity of mixed CACC vehicle traffic to set the demand inputs for mainline generators, we conducted simulations on an 11 km long section with four lanes, identical to the network in Fig. 4 except the on-ramp. Similarly, the CACC MPR varies from 0% to 100% by a 20% interval. The capacity was estimated by slowly increasing the traffic demand until the generated vehicles are held at the beginning of the network. The demand was increased by 100 veh/h/lane. The throughput was collected by a group of detectors located at 10 km downstream. The 5-min flow data was aggregated into a 15-min data and the average of the maximum 15-min throughput from five cases is denoted as the pipeline capacity (HCM, 2000).

4. Results

In this section, the fundamental diagrams of mixed CACC vehicle traffic flow are firstly presented, giving a general overview of the

Table 2
Typical values of parameters used in simulation.

Parameters	Typical value
Conventional vehicles (IDM +)	
Maximum acceleration a	1.25 m/s²
Maximum deceleration b	2.09 m/s²
Stopping distance s0	3 m
Shared with conventional vehicles and CACC vehicles	
Desired time gap under manual driving	1.4 s
Vehicle length	4 m
Free-flow speeds	N (125, 8.75) km/h
Only for CACC vehicles	
V2V communication range	300 m
Sensor range	120 m
Desired time gap under ACC	1.1 s
Desired time gap under CACC	0.6 s (57%), 0.7 s (24%), 0.9 s (7%), 1.1 s (12%)
CACC inter-string gap	1.5 s
CACC string length limit	10 vehicles
ACC-CACC lower acceleration limit	− 4 m/s²
ACC-CACC upper acceleration limit	2 m/s²

changes in traffic characteristics e.g. capacity and data scattering. It is followed by a table of capacities including the theoretical capacity upper bound, pipeline capacity and merging capacity, analysed with the CACC MPR and CACC time usage. After that, we pay attention to the capacity drop and investigate the causes of the capacity drop in terms of CACC deactivation, and lastly we show the interaction between CACC deactivation and large following gaps by vehicle trajectory data.

4.1. Fundamental diagram

Fig. 5 shows the flow-density and speed-density relationship at the merging bottleneck with an increased CACC MPR, deriving from detectors at D1 using section-based flow and harmonic speed. As observed, the general shape of the fundamental diagram does not show clear changes with the appearance of CACC vehicles: the flow-density plots follow the reverse-λ curve described in Wu (2002) for manually-driven vehicle traffic, unlike the triangular fundamental diagram assumed in Bose and Ioannou (2003) and Levin and Boyles (2016) for automated vehicle traffic. A discontinuity between the free-flow regime and congested-flow regime, which is an implication of capacity drop, is the characteristic of a reverse-λ fundamental diagram as opposed to the triangular fundamental diagram. Therefore, the above flow-density plots suggest the existence of the capacity drop in mixed traffic with conventional vehicles and CACC vehicles (Treiber et al., 2006). Another characteristic that remains unchanged is the free-flow speed in the speed-density plot. The reason behind the unchanged free-flow speed is that the intended speeds of CACC vehicles follow the same distribution of intended speeds of conventional vehicles.

One noticeable change in the flow-density plots is that the data points are more scattered as usual in the congested-flow regime than the free-flow regime, and the scatter increases with CACC MPRs. The scatters can be largely attributed to different operational modes (cruising, gap-closing and gap-regulating) of ACC and CACC, as well as the vehicle controls switching among human driver, ACC and CACC system, which essentially increase the heterogeneity of road user behaviours. Moreover, the string instability of the ACC car-following model can be another explanation for the scattering. The amplified overshoot in the ACC following response has been shown in Milanes and Shladover (2014) in both field tests and simulations, and it may create shock waves that cause largely scattered data in congested flow. This finding is different from previous studies (Talebpour and Mahmassani, 2016) which suggested that the scatter in the fundamental diagram decreases as MPR of automated vehicles (using the CACC algorithm by van Arem et al. (2006)) increases from 50% to 100%. In Talebpour and Mahmassani (2016), a single-lane simulation was conducted with a mainline flow of 1800 veh/h and on-ramp demand set as 360 veh/h, which barely reaches the capacity at high MPRs of automated vehicles. The observed data located only in the free-flow regime and the scatter in the fundamental diagram naturally decreased, compared to the low MPRs case where data were also observed in the congested-flow regime. Apart from the different demand level, the different driving modes and authority transitions of CACC system were not modelled in Talebpour and Mahmassani (2016). That resulted in a more homogeneous and equilibrium flow state compared to our simulation.

4.2. Theoretical capacity upper bound, pipeline capacity and merging capacity

From the fundamental diagrams, the changes in throughput with the increase of CACC vehicles are clearly observed. Table 3 lists the theoretical upper bounds for the roadway capacity, and the simulated capacities at each CACC MPR for the pipeline network and merging bottleneck, with increases compared to the 0% CACC reference case. The theoretical capacity upper bound is calculated based on the probability of each vehicle class follow the other vehicle class and corresponding time gap settings, as well as the vehicle length and vehicle percentage, assuming the critical speed is 100 km/h (observed from the Fig. 5b). The bounds give an indication on the maximum possible throughput when traffic is in equilibrium state.

The theoretical capacity upper bound, pipeline capacity and merging capacity exhibit a marginal increase at low CACC MPRs and a large increase at high CACC MPRs. The marginal increase at low CACC MPRs can be explained by the low time usage of the CACC system. The ad hoc clustering probability of two CACC vehicles is approximately the squared vehicle market penetration rates, which is very small at low MPRs. Since the CACC system is only activated when another CACC vehicle is found directly in front, most of CACC vehicles actually travel under ACC operation instead of CACC operation at low MPRs, with a time gap larger than CACC settings but smaller than that of a human driver. Similarly, the strong increase of capacity at high CACC MPRs is the result of increased CACC operation. As the CACC vehicle propotion increases, the clustering probability increases strongly and thus more vehicles operate in CACC system, so that the throughput is enhanced by small car-following time gaps.

Although the increasing trends are similar, discrepancies exist among the theoretical capacity, pipeline capacity and merging capacity. In 100% CACC vehicles scenario, the theoretical upper bound is around 3877 veh/h/lane, while the value decreases slightly to 3824 veh/h/lane for pipeline capacity and dramatically to 3293 veh/h/lane for merging capacity. First of all, the theoretical upper bound is the highest value at each CACC MPR as the equilibrium traffic flow was estimated. Regardless of the traffic dynamics and lane change behaviour, the theoretical capacity shows the greatest potential of CACC vehicles for throughput increase in an ideal situation. The merging capacity is lower than the pipeline capacity at all CACC MPRs as disturbances are introduced by the bottleneck. Due to many lane changes in the vicinity of the bottleneck, CACC systems degrade to ACC or human-driven modes with larger gaps, which result in a reduction in throughput. Because the pipeline capacity does not include disturbance at realistic traffic networks, it tends to overestimate the capacity of highways with CACC system. The merging capacity shows a more achievable and reliable potential of CACC vehicles in a realistic traffic network.

Since the increase of capacity is closely related to the operation of the CACC system, we investigate the relation between the merging capacity and the CACC operation ratio illustrated in Fig. 6a. The CACC operation ratio is given as the ratio of time that the system operates in CACC mode over the time of all vehicles, analysed from the vehicle trajectories at the merging bottleneck
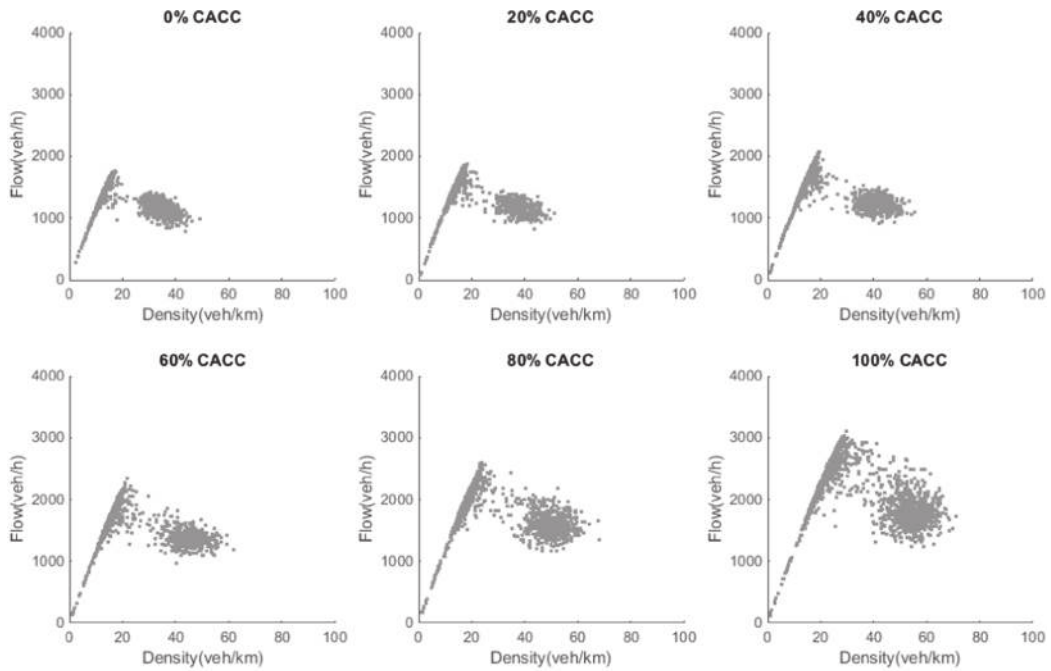
(a) Flow-Density plots with CACC MPRs
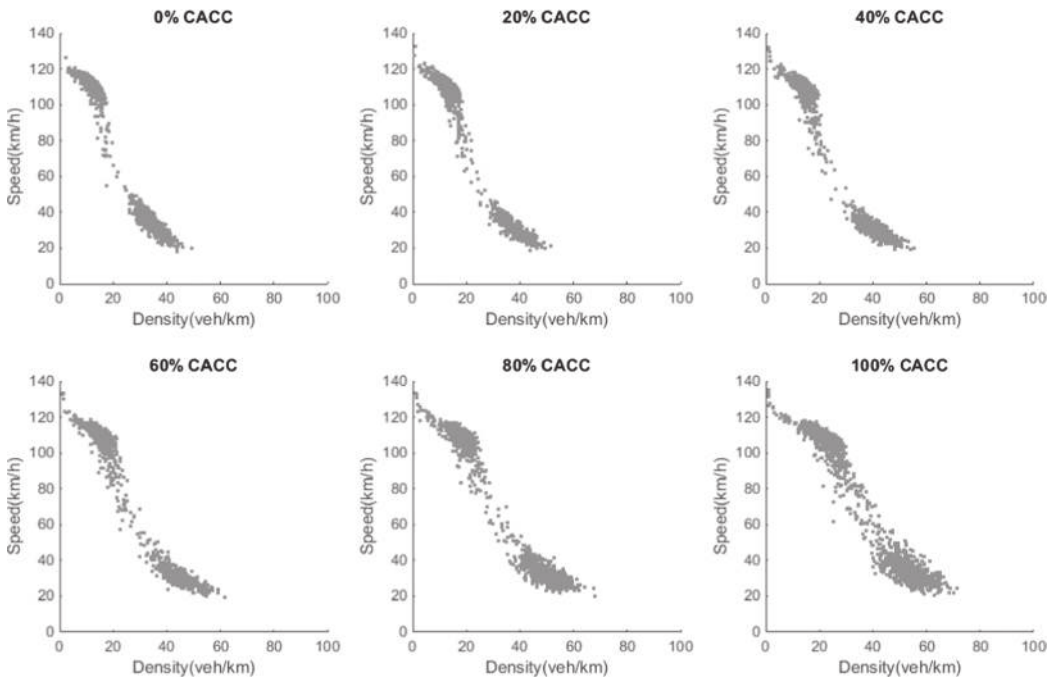
(b) Speed-Density plots with CACC MPRs

Fig. 5. Fundamental diagrams at merging bottleneck (Detector D1) at different CACC market penetration rates.

(7950–8050 m). The merging capacity is found as a quadratic function of the CACC operation ratio and in fact the actual CACC operation ratios are far below the corresponding CACC MPRs. In Fig. 6b, a bar plot of vehicle percentage in time under CACC, ACC and human driver control (deactivated) is provided to explain the operation states of CACC vehicles with the vehicle percentage of

Table 3

Free-flow capacity and queue discharge rate with CACC market penetration rates, compared to theoretical upper bound and the pipeline capacity.

| veh/h/lane	CACC market penetration rates					
	0%	20%	40%	60%	80%	100%
Theoretical upper bound	2332	2452	2645	2945	3397	3877
Pipeline capacity	2124	2222	2353	2620	3092	3824
Δ	–	4.6%	10.8%	23.3%	45.6%	80.1%
Merging capacity	2031	2094	2197	2400	2708	3293
Δ	–	3.1%	8.2%	18.2%	33.3%	62.1%
Queue discharge Flow	1684	1774	1837	1999	2268	2725
Δ	–	5.3%	9.1%	18.7%	43.3%	61.8%
Capacity drop	347	320	360	401	440	568
%	17.1%	15.4%	16.4%	16.7%	16.0%	17.2%
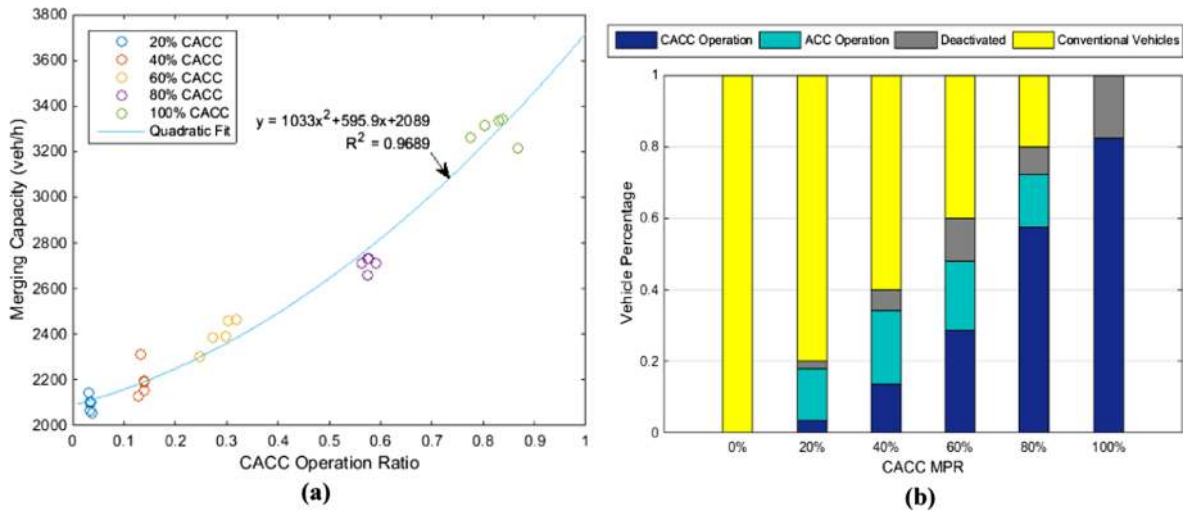
Fig. 6. (a) a relation between merging capacity and CACC operation ratio (b) vehicle percentage in CACC operation with CACC MPRs, based on trajectory data collected from the 7950–8050 m section.

conventional vehicles. The results show that in mixed CACC vehicle flow, a considerable percentage of CACC vehicles are operated under ACC, while a certain percentage of CACC is deactivated and under manual driving at the merging bottleneck. For instance, at the 20% CACC MPR, only 3.5% of vehicles are operated by CACC, while 14.3% of vehicles are operated under ACC and a 2.2% of vehicles are operated in the manually driven mode. As the CACC MPR increases, the percentage of CACC operation increases and that of ACC operation decreases, contributing to a much higher usage of CACC at high MPRs.

The percentage of deactivated CACC systems generally increases with CACC MPRs, from 2.2% at 20% CACC MPR to 17.5% in the 100% CACC case. The deactivated CACC operation, which is mainly due to the lane-change-related deactivation at the merge, leaves a gap between the ideal CACC usage and the actual CACC usage at the bottleneck. Thus, it is an important explanation for the discrepancies between pipeline capacity and merging capacity in Table 3. As it increases with CACC MPRs, the discrepancy increases because there are more CACC deactivations due to lane changes. This further hinders the potential of CACC systems in increasing capacity of a merging bottleneck.

4.3. Capacity drop and CACC deactivation

Table 3 lists the queue discharge flow at each CACC MPR from the scenario that the averaged throughput in congestion is the highest at different on-ramp demands. The queue discharge flow shows a similar increasing trend with the merging capacity that there is a small increase at low CACC MPRs and a fast increase at high CACC MPRs.

The difference between the merging capacity and queue discharge rate is referred as a capacity drop (Yuan et al., 2017). In Table 3, it ranges from 320 to 586 veh/h/lane and generally increases with CACC MPRs. The capacity drop for conventional vehicle traffic is 17.1%, and it varies between 15.4% and 17.2% for traffic with CACC vehicles. The results suggest that the capacity drop in CACC traffic exists and its extent is comparable to that in conventional vehicular traffic.

According to the relation between the capacity/throughput and CACC usage, it is reasonable to investigate the capacity drop in terms of CACC deactivation. In Table 4, we retrieve the time ratios of different operation modes from vehicle trajectories at the merging bottlenck (7950–8050 m) when the merging capacity and queue discharge rates are measured. The comparison of operation

Table 4

Operation ratios of CACC, ACC and manual driving (deactivated) in the free-flow capacity case and queue discharge rate case at the merging bottleneck.

Operation	CACC MPR				
	20%	40%	60%	80%	100%
CACC	3.5%/2.8%	13.6%/9.9%	28.8%/22.4%	57.6%/39.5%	82.3%/57.8%
ACC	14.3%/10.8%	20.7%/14.6%	19.3%/14.3%	14.6%/9.0%	0.2%/0.1%
Deactivated	2.2%/6.4%	5.7%/15.5%	11.9%/23.4%	7.8%/31.5%	17.5%/42.2%

Note: CACC operation ratios in free-flow capacity case/CACC operation ratios in quque discharge rate case.

ratios in such two cases shows decreases in the CACC and ACC operation time, but an increase time ratio of deactivation at all CACC MPRs. It suggests that more CACC are deactivated, either from ACC or CACC operation, at the merging bottleneck after traffic breakdown. In fact, at CACC MPRs below 40%, the increased ratio of deactivated CACC come from more ACC than CACC operation, while at high MPRs above 60%, more CACC operation than ACC operation is deactivated. Since the time gap of CACC is much smaller than that of the ACC, the change of car-following time gap from CACC operation is larger than that from ACC operation. For this reason, a higher CACC MPR leads to a larger throughput in the capacity drop, explaining the similar deactivated CACC ratio in 80% and 100% but with a different capacity drop in vehicle number.

At the macroscopic level, a relation in space and time exists between the congestion pattern and the number of deactivations. The number of deactivations refers to the instance that the CACC system switches to the manual driving within a 5-min time interval in a 1-km section, and it includes the multiple deactivations of a CACC vehicle. One simulation run of 60% CACC with 1200 veh/h on-ramp demand is shown as an example in Fig. 7. At the merging section (8–9 km) and its upstream section, the increase of the number of deactivations shows a consistent time-space pattern with the traffic congestion shown as speed and flow reduction in Fig. 7a and c. The speed reduction at the merging bottleneck appears at 28 min and the number of deactivation starts to dramatically increase at the same time and location. When the congestion propagates to upstream sections, the number of deactivations in the upstream section also increases, showing a strong interaction between the traffic congestion and number of deactivations. In addition, the capacity drop before and after traffic breakdown is clearly observed in Fig. 7c.

Fig. 8 shows the relationship between the traffic flow speed and number of deactivations per km·5-min. As it is clearly observed, the number of deactivation is below 50 at high speeds above 80 km/h and it dramatically increases to a large number between 100 and 200 at speeds around 30 km/h. The deactivations at high speeds are found related to the lane changes for merging traffic and the deactivations at low speeds are the results of collision warning during the shock waves in congestion propagation. In this regard, this figure implies a mutual interaction between the traffic congestion, capacity drop and CACC deactivation.

4.4. Verification by vehicle trajectory

CACC system deactivation results in switches among control systems and operational modes that lead to larger vehicle gaps. Under CACC mode, CACC vehicles maintain a gap no larger than 1.1 s, but the desired gap of human-driven vehicles is 1.4 s. System deactivation inevitably causes an increase of time gap, which corresponds to a lower flow. Fig. 9a presents the equilibrium gap-speed relationship under different operating modes, from the rightmost lane of a simulation run with 60% CACC and 1200 veh/h on-ramp
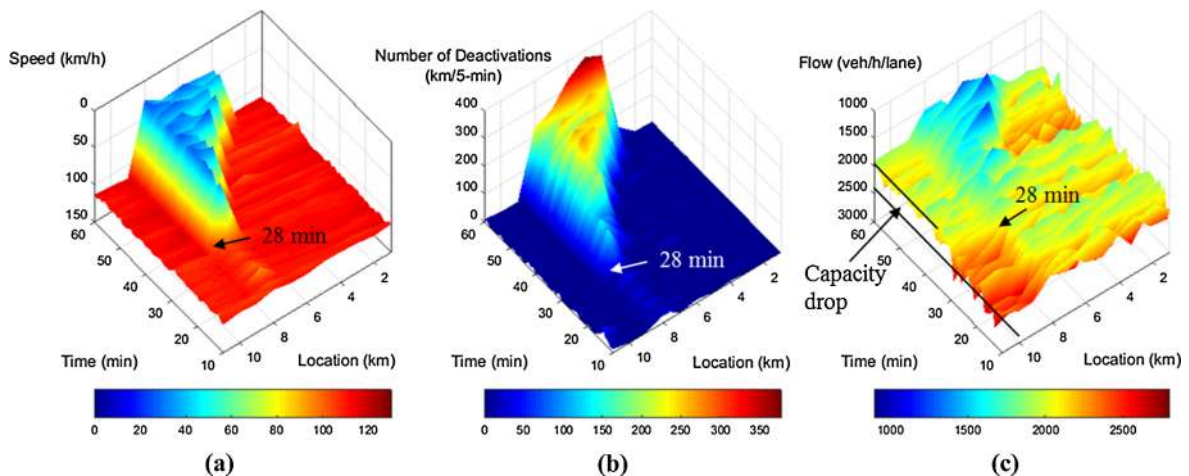

Fig. 7. The relations among congestion pattern and number of deactivations. An example in the 60% CACC scenario with a 1200 veh/h on-ramp demand.
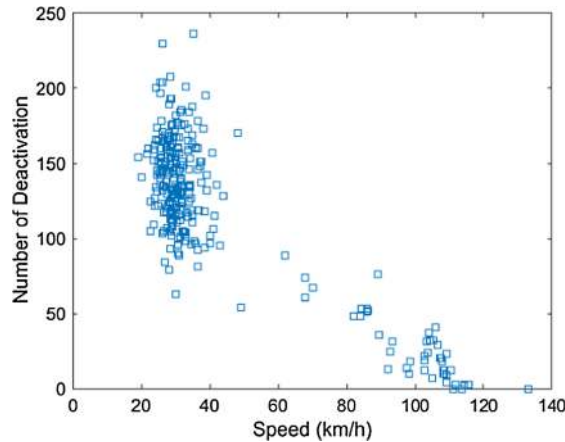
Fig. 8. Plot of speed reduction and numbers of deactivation within 8–9 km. Data from simulation runs of the 60% CACC scenario with a 1200 veh/h on-ramp demand.
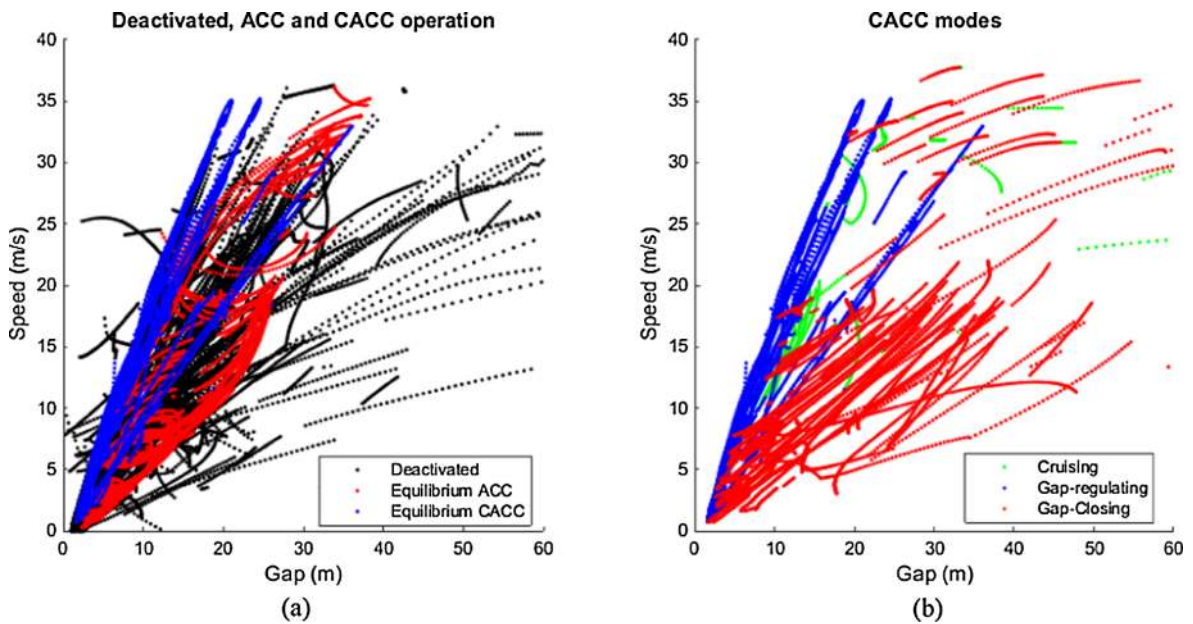

Fig. 9. The speed-gap plot for manual driving, equilibrium ACC and equilibrium CACC operation (a); The speed-gap plot for cruising, gap-regulating and gap-closing mode under CACC operation (b).

demand. The vehicle trajectories were collected within 7–9 km for the whole simulation period, and the equilibrium state refers to the condition that a CACC vehicle is operated in the gap-regulating mode. Firstly, it is evident that the CACC has a shorter following gap than ACC in equilibrium state and also than manual driving. Secondly, vehicles under CACC perform more stable following behaviour than vehicles under ACC and manual driving, shown as the less scattered gap-speed observations in each desired time gap setting under CACC mode than the observations under the other modes. This pattern will prevail with different CACC MPRs since the equilibrium states under ACC and CACC are only related to their car-following models and time gap settings.

A secondary consequence of CACC deactivation appears after the CACC system is reactivated. Immediately after the re-activation, most CACC vehicles are operated in gap-closing mode, since the gap is too large to implement the gap-regulating mode. The gap-closing mode gradually reduces the time gap until the switching threshold of gap-regulation mode is met. As can be seen from the speed-gap plot in Fig. 9b, the gaps under gap-closing mode are larger than the gap-regulating mode, coresponding to a low throughput after the reactivation. Fig. 9 establishes a connection between the microscopic vehicle behaviour and macroscopic traffic flow, points out the changes in flow state after CACC deactivation and gives an insight into the impacts of the switches among control systems and driving modes.

In addition to the speed-gap plot, vehicle trajectories provide evidence of increased following gaps due to the deactivation of CACC. In Fig. 10, the trajectories near the merging point of two CACC vehicles, from the rightmost lane of a simulation run with 60% CACC and 1200 veh/h on-ramp demand, are highlighted and marked as 1 and 2. For each of them, a virtual trajectory is plotted
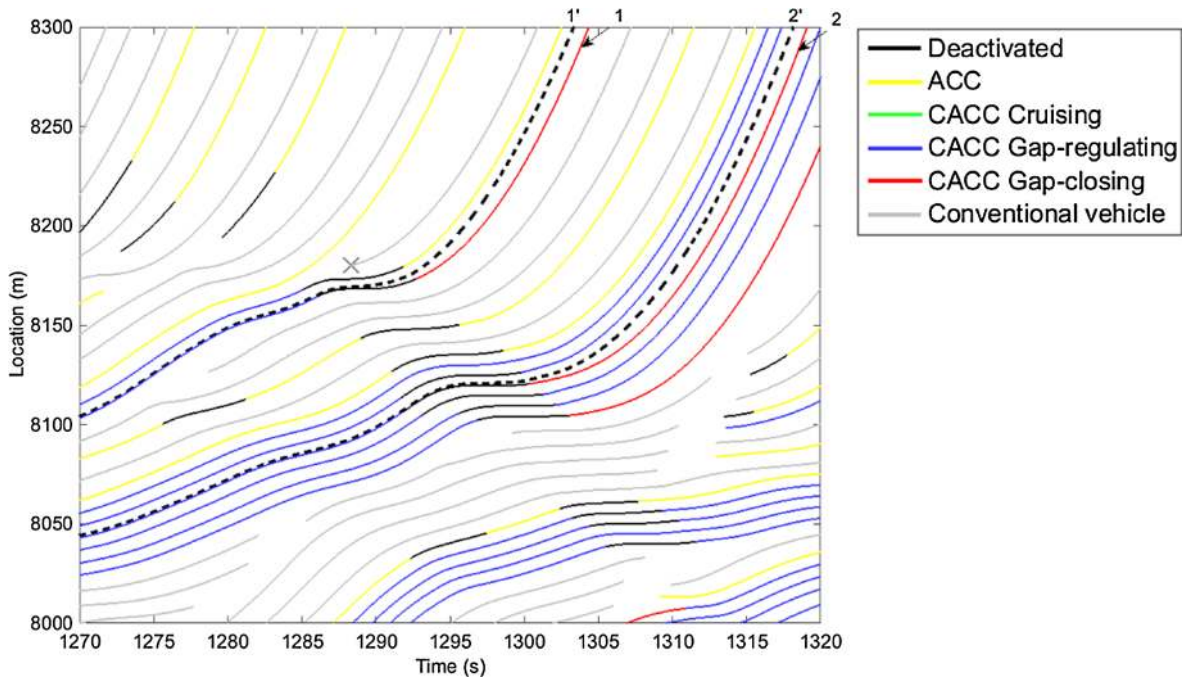
Fig. 10. Virtual CACC vehicle trajectories showing the increased large following gaps by CACC deactivation.

(marked as 1′ and 2′) as a dashed line using the speed of the leader at each time step and by calculating the position of the virtual CACC follower assuming the CACC vehicle were not deactivated. These two pairs of vehicle trajectories present the deactivation of CACC string followers during a shock wave caused by a merging vehicle (marked as a cross). Before the deactivation, they are all in CACC gap-regulating mode and they enter the gap-closing mode after the CACC resumes control, which results in a larger gap than the gap-regulating mode as shown by the virtual trajectories. In combination with the speed-gap plots, we present evidence of increased time gaps after CACC deactivations caused not only by the different desired time gap settings between ACC, CACC and manual driving, but also by the changes in driving mode in CACC systems.

5. Discussion

Our study shows several new insights into the traffic flow characteristics with CACC vehicles. One interesting finding is that introducing CACC vehicles into manually driven vehicle traffic does not change the inverse-λ shape of fundamental diagram. The free-flow regime and congested-flow regime are clearly observed, and they retain their characteristics with a discontinuity between two regimes. The results imply the existence of a two-capacity phenomenon in mixed CACC vehicle flow, which has been widely observed in conventional vehicle traffic but has not previously been discussed in CACC studies.

Another important finding is that CACC vehicles increase the roadway capacity both at road segments and merging bottlenecks, with a trend of a small increase at low CACC MPRs (20–40%) and a strong increase at high CACC MPRs (60–100%). These results are in line with those of previous studies (van Arem et al., 2006, Shladover et al., 2012, VanderWerf et al., 2002, Tientrakool et al., 2011). Moreover, we found that the increase in throughput is not only related to the CACC MPRs, but also to the probability of two CACC vehicles being clustered and the system deactivations due to lane changes. For a more direct and accurate description, the capacity is closely related to the time usage of activated CACC operation, a consequence of realized ACC/CACC time gaps determined by CACC MRPs.

In addition, the deactivation of CACC is found as an important factor in reducing the capacity at the merging bottleneck compared to the pipeline capacity. It also contributes to the capacity drop. As CACC MPR increases, the influence of a bottleneck with network heterogeneity becomes stronger because of a higher percentage of CACC deactivation caused by (mandatory) lane changes. The capacity drop in vehicle per hour increases with CACC MPRs but it does not strongly vary by percentage in throughput. The number of CACC deactivations is found to be consistent with the congestion pattern in time and location, and is related to the speed of traffic flow. The capacity drop in mixed CACC vehicle traffic has not been investigated previously and our study provides new insights into the relation between the capacity drop and CACC deactivations.

These findings may help vehicle manufacturers to refine or even redesign their systems to improve traffic flow performance. Vehicle manufacturers should work on increasing the operational design domain of ACC/CACC systems such that they can handle more traffic situations such as safety-critical situations and low speed operations, to reduce the number of system deactivation. In addition, with the use of V2V connectivity, the merging vehicles and vehicles in the mainline could work in a more coordinated way, which could potentially increase the capacity at a merging bottleneck (Milanés and Shladover, 2015, Wang et al., 2015). The

enhanced system functionalities can improve the resilience of traffic flow and further increase the merging capacity.

The insights into traffic flow characteristics from our simulations also have implications for highway traffic management. It is noteworthy for road operators that the capacity benefit of CACC systems should be evaluated at highway bottlenecks and at low MPRs the potential of CACC systems is marginal due to the low probability of CACC vehicles following each other. Increasing the activated CACC operation ratio is more effective than increasing the CACC vehicle MPR in terms of improving the traffic flow operation. Especially at the early stage of implementing CACC, road operators may explore strategies in either increasing the clustering probability of CACC vehicles, such as a dedicated lane operation and active platooning strategy, or increasing the number of vehicles equipped with V2V communication. Another paradigm of highway management strategies involves the use of Infrastructure-to-Vehicle (I2V) communications connecting traffic control with vehicle control systems to harmonize traffic flow or resolve stop-and-go traffic, which will potentially reduce the system deactivations. This has shown to be effective in simulations (Roncoli et al., 2016, Wang et al., 2016a, Baskar et al., 2012).

Our study focuses on the merging bottleneck but the findings also bear significance for other bottlenecks such as weaving section and lane drops. In a weaving section, there is additional exiting traffic that interacts with the mainline and merging traffic within a short section, which often leads to a larger speed reduction than a merging bottleneck. For CACC vehicles taking exits, more deactivations are anticipated due to the lane change requests for following routes, and the influence of system deactivation is therefore expected to be stronger compared to a merging bottleneck. This expectation is consistent with Hartmann et al. (2017), concluding that the capacity of mixed CACC traffic at weaving sections is lower than the merging bottleneck. In a lane drop scenario, vehicles have to change lane to follow the route similar to the merging bottleneck scenario, but the lane changes could be performed at upstream sections in advance whenever the gap is available and thus less deactivations of CACC happen in the mainline for cooperative lane changes. In this way, the negative impacts of a lane drop bottleneck will be less than that of the merging bottleneck.

It should be noted that our assumptions on CACC activation and deactivation might not be complete. For example, our model does not include the deactivation for courtesy lane changes, during which the courtesy provider might actively deactivate the system to yield gap for the lane changer. On the other hand, drivers with activated CACC might be less inclined to provide cooperation or courtesy, resulting in fewer CACC deactivations.

6. Conclusion and outlook

In this paper, we formulated the extension of a realistic CACC behaviour model with system deactivation/reactivation and a string length constraint, which are essential determinants of roadway capacity. The CACC model was implemented in the simulation model MOTUS, with which we conducted simulations to investigate impacts of CACC vehicles on traffic flow characteristics at a merging bottleneck, particularly on the fundamental diagram and roadway capacity.

Our work reveals that there are some noticeable changes in the fundamental diagram, especially, a wider spread of traffic states in the congested branch of the fundamental diagram with the increase of CACC MPRs. This is explained by the multi-regime nature of the full-speed-range CACC controllers and the degradation of CACC to ACC and human-driven modes.

The simulation results show that roadway capacity increases with CACC MPRs both on homogeneous highway sections and merging bottlenecks, up to 3824 veh/h/lane and 3293 veh/h/lane respectively for a four-lane highway with 100% CACC vehicles. The pipeline capacity and merging capacity both exhibit a slow increase at CACC MPRs below 40% and a rapid increase at CACC MPRs above 60%. The merging capacity is 6% −14% lower than the pipeline capacity at the same CACC MPR since the merging disturbances greatly limit the flow increase by the increased CACC MPRs. Drivers have to take over vehicle control to enable cooperative lane changes, and that significantly compromises the capacity benefits of CACC systems.

The capacity drop at merging bottleneck is explained by the CACC deactivation, which increases the time gap between CACC vehicles and their predecessors consequently. After traffic congestion appears, the number of deactivations increases substantially due to safety concerns and lane change requests, which leads to a larger number of vehicle control switches from CACC to manual driving and from gap-regulating mode to gap-closing mode after CACC reactivation. The changes among multiple vehicle operations and modes result in large time gaps and thus lead to a capacity drop.

The capacity drop can be further investigated by CACC deactivation types. Future research can focus on segregating the effect of each deactivation type on reducing throughput at different traffic bottlenecks, i.e. merging, splitting, weaving and lane drop. Other than roadway capacity, special attention can be paid to string stability of the proposed CACC car-following model. The discrete-time property, multi-regime state and the inclusion of historical vehicle state pose challenges to the string stability analysis. Deactivation in approaching scenarios can potentially be reduced by including a quadratic term of relative speed in the approaching model, which makes the model nonlinear. Moreover, future study points to the extension of CACC simulations of highway corridors with multiple interacting bottlenecks to see the impacts of CACC vehicles in mitigating congestion. In addition, the considerable capacity drop due to CACC deactivation suggests a need for developing a better strategy for CACC vehicle cooperation or coordination at merging sections. Future study will pay attention to the cooperative merging control to further boost the roadway capacity by CACC vehicles. Besides, lane management strategies such as a CACC vehicle dedicated lane can be used to maximize the positive effects of CACC vehicles in low MPRs and it remains as an interesting topic to be studied. Learning-based car-following models that capture more historical information and provide higher prediction capability (Zhou et al., 2017, Wang et al., 2018) could be applied to model future CACC vehicles, and impact assessment of such systems on traffic flow is also a nice topic to be explored.

Acknowledgment

References

Arnaout, G., Bowling, S., 2011. Towards reducing traffic congestion using cooperative adaptive cruise control on a freeway with a ramp. J. Ind. Eng. Manage. 4, 699–717.

Arnaout, G.M., Arnaout, J.P., 2014. Exploring the effects of cooperative adaptive cruise control on highway traffic flow using microscopic traffic simulation. Transport. Plan. Technol. 37, 186–199.

Banks, J.H., 1991. The two-capacity phenomenon: some theoretical issues. Transp. Res. Rec. 234–241.

Baskar, L.D., de Schutter, B., Hellendoorn, H., 2012. Traffic management for automated highway systems using model-based predictive control. IEEE Trans. Intell. Transp. Syst. 13, 838–847.

Bose, A., Ioannou, P., 2003. Mixed manual/semi-automated traffic: a macroscopic analysis. Transport. Res. C: Emerg. Technol. 11, 439–462.

Calvert, S.C., Broek, T.H.A.V.D., Noort, M.V., 2011. Modelling cooperative driving in congestion shockwaves on a freeway network. In: 14th International IEEE Conference on Intelligent Transportation Systems, 2011 Washington, DC.

Chen, D.J., Ahn, S., Chitturi, M., Noyce, D.A., 2017. Towards vehicle automation: roadway capacity formulation for traffic mixed with regular and automated vehicles. Transport. Res. B – Methodol. 100, 196–221.

Ge, J.I., Orosz, G., 2017. Optimal control of connected vehicle systems with communication delay and driver reaction time. IEEE Trans. Intell. Transp. Syst. 18, 2056–2070.

Ghiasi, A., Hussain, O., Qian, Z., Li, X., 2017. A mixed traffic capacity analysis and lane management model for connected automated vehicles: a Markov chain method. Transport. Res. B: Methodol. 106, 266–292.

Guériau, M., Billot, R., el Faouzi, N.-E., Monteil, J., Armetta, F., Hassas, S., 2016. How to assess the benefits of connected vehicles? A simulation framework for the design of cooperative traffic management strategies. Transport. Res. C: Emerg. Technol. 67, 266–279.

Hall, R.W., Li, C., 1999. Lane capacity for an automated highway with mixed vehicle classes. ITS J. – Intell. Transport. Syst. J. 5, 217–240.

Hartmann, M., Motamedidehkordi, N., Krause, S., Hoffmann, S., Vortisch, P., Busch, F., 2017. Impact of automated vehicles on capacity of the German freeway network. ITS World Congress Montreal.

HCM, 2000. Highway Capacital Manual. Transportation Research Board, Washington, D.C.

Ioannou, P.A., 1997. Automated Highway Systems. Springer, US.

Kanaris, A., Ioannou, P., Ho, F.S., 1997. Spacing and capacity evaluations for different AHS concepts. In: Proceedings of the 1997 American Control Conference, vols. 1–6, 2036–2040.

Kesting, A., Treiber, M., Helbing, D., 2010. Enhanced intelligent driver model to access the impact of driving strategies on traffic capacity. Philos. Trans.: Math. Phys. Eng. Sci. 368, 4585–4605.

Kesting, A., Treiber, M., Schönhof, M., Helbing, D., 2008. Adaptive cruise control design for active congestion avoidance. Transport. Res. C: Emerg. Technol. 16, 668–683.

Kiefer, R.J., Leblanc, D.J., Flannagan, C.A., 2005. Developing an inverse time-to-collision crash alert timing approach based on drivers' last-second braking and steering judgments. Accid. Anal. Prev. 37, 295–303.

Klunder, G., Li, M., Minderhoud, M., 2009. Traffic flow impacts of adaptive cruise control deactivation and (re)activation with cooperative driver behavior. Transport. Res. Rec.: J. Transport. Res. Board 145–151.

Levin, M.W., Boyles, S.D., 2016. A multiclass cell transmission model for shared human and autonomous vehicle roads. Transport. Res. C-Emerg. Technol. 62, 103–116.

Liu, H., Kan, X., Shladover, S.E., Lu, X.-Y., Ferlis, R.E., 2018a. Impact of cooperative adaptive cruise control on multilane freeway merge capacity. J. Intell. Transport. Syst. 22, 263–275.

Liu, H., Kan, X., Shladover, S.E., Lu, X.-Y., Ferlis, R.E., 2018b. Modeling impacts of cooperative adaptive cruise control on mixed traffic flow in multi-lane freeway facilities. Transport. Res. C: Emerg. Technol. 95, 261–279.

Makridis, M., Mattas, K., Ciuffo, B., Raposo, M.A., Thiel, C., 2017. Assessing the impact of connected and automated vehicles. A freeway scenario. In: Zachäus, C., Müller, B., Meyer, G. (Eds.) Advanced microsystems for automotive applications 2017. Lecture Notes in Mobility. Springer, Cham.

Michael, J.B., Godbole, D.N., Lygeros, J., Sengupta, R., 1998. Capacity analysis of traffic flow over a single-lane automated highway system. ITS J. – Intell. Transport. Syst. J. 4, 49–80.

Milanes, V., Shladover, S.E., 2014. Modeling cooperative and autonomous adaptive cruise control dynamic responses using experimental data. Transport. Res. C-Emerg. Technol. 48, 285–300.

Milanés, V., Shladover, S.E., 2015. Handling cut-In vehicles in strings of cooperative adaptive cruise control vehicles. J. Intell. Transport. Syst. 20, 178–191.

Milanés, V., Shladover, S.E., Spring, J., Nowakowski, C., Kawazoe, H., Nakamura, M., 2014. Cooperative adaptive cruise control in real traffic situations. IEEE Trans. Intell. Transp. Syst. 15, 296–305.

Nowakowski, C., Shladover, S.E., Cody, D., Bu, F., O'Connell, J., Spring, J., Dickey, S., Nelson, D., 2011. Cooperative adaptive cruise control: testing drivers' choices of following distances. Institute of Transportation Studies, University of California at Berkeley, California PATH Program.

Pauwelussen, J., Feenstra, P.J., 2010. Driver behavior analysis during ACC activation and deactivation in a real traffic environment. IEEE Trans. Intell. Transp. Syst. 11, 329–338.

Pauwelussen, J., Minderhoud, M., 2008. The effects of deactivation and (re)activation of ACC on driver behaviour analyzed in real traffic. IEEE Intelligent Vehicles Symposium. Eindhoven, The Netherlands. IEEE, pp. 257–262.

Rajamani, R., Choi, S.B., Law, B.K., Hedrick, J.K., Prohaska, R., Kretz, P., 2000. Design and experimental implementation of longitudinal control for a platoon of automated vehicles. J. Dyn. Syst. Measur. Control-Trans. ASME 122, 470–476.

Roncoli, C., Papamichail, I., Papageorgiou, M., 2016. Hierarchical model predictive control for multi-lane motorways in presence of Vehicle Automation and Communication Systems. Transport. Res. C: Emerg. Technol. 62, 117–132.

Schakel, W.J. MOTUS [Online]. Available: < http://homepage.tudelft.nl/05a3n/ > [Accessed April, 25 2015].

Schakel, W.J., Knoop, V.L., van Arem, B., 2012. Integrated lane change model with relaxation and synchronization. Transport. Res. Record: J. Transport. Res. Board 47–57.

Schakel, W.J., Van Arem, B., Netten, B.D., 2010. Effects of cooperative adaptive cruise control on traffic flow stability. In: 13th International IEEE Annual Conference on Intelligent Transportation Systems, 2010 Madeira Island, Portugal. IEEE, pp. 759–764.

Shladover, S.E., Nowakowski, C., Lu, X.Y., Ferlis, R., 2015. Cooperative adaptive cruise control: definitions and operating concepts. Transp. Res. Rec. 145–152.

Shladover, S.E., Su, D., Lu, X.-Y., 2012. Impacts of cooperative adaptive cruise control on freeway traffic flow. Transport. Res. Record: J. Transport. Res. Board 63–70.

Swaroop, D., Hedrick, J.K., Chien, C.C., Ioannou, P., 1994. A comparision of spacing and headway control laws for automatically controlled vehicles. Veh. Syst. Dyn. 23, 597–625.

Talebpour, A., Mahmassani, H.S., 2016. Influence of connected and autonomous vehicles on traffic flow stability and throughput. Transport. Res. Part C – Emerg. Technol. 71, 143–163.

Tientrakool, P., Ho, Y.C., Maxemchuk, N.F., 2011. Highway capacity benefits from using vehicle-to-vehicle communication and sensors for collision avoidance. 2011

IEEE Vehicular Technology Conference (Vtc Fall).

Tilg, G., Yang, K., Menendez, M., 2018. Evaluating the effects of automated vehicle technology on the capacity of freeway weaving sections. Transport. Res. C: Emerg. Technol. 96, 3–21.

Treiber, M., Hennecke, A., Helbing, D., 2000. Congested traffic states in empirical observations and microscopic simulations. Phys. Rev. E 62, 1805–1824.

Treiber, M., Kesting, A., Helbing, D., 2006. Understanding widely scattered traffic flows, the capacity drop, and platoons as effects of variance-driven time gaps. Phys. Rev. E Stat. Nonlin. Soft. Matter. Phys. 74, 016123.

van Arem, B., van Driel, C.J.G., Visser, R., 2006. The impact of cooperative adaptive cruise control on traffic-flow characteristics. IEEE Trans. Intell. Transp. Syst. 7, 429–436.

Vanderwerf, J., Shladover, S.E., Kourjanskaia, N., Miller, M., Krishnan, H., 2001. Modeling effects of driver control assistance systems on traffic. Transport. Res. Rec.: J. Transport. Res. Board 167–174.

Vanderwerf, J., Shladover, S.E., Miller, M.A., Kourjanskaia, N., 2002. Effects of adaptive cruise control systems on highway traffic flow capacity. Transport. Res. Record: J. Transport. Res. Board 78–84.

Varotto, S.F., Hoogendoorn, R.G., van Arem, B., Hoogendoorn, S.P., 2015. Empirical longitudinal driving behavior in authority transitions between adaptive cruise control and manual driving. Transport. Re. Record: J. Transport. Res. Board 2489, 105–114.

Viti, F., Hoogendoorn, S.P., Alkim, T.P., Bootsma, G., 2008. Driving behavior interaction with ACC: results from a field operational test in the Netherlands. 2008 IEEE Intelligent Vehicles Symposium 1–3, 444–449.

Wang, M., Daamen, W., Hoogendoorn, S.P., van Arem, B., 2016a. Connected variable speed limits control and car-following control with vehicle-infrastructure communication to resolve stop-and-go waves. J. Intell. Transport. Syst. 20, 559–572.

Wang, M., Daamen, W., Hoogendoorn, S.P., van Arem, B., 2016b. Cooperative car-following control: distributed algorithm and impact on moving jam features. IEEE Trans. Intell. Transp. Syst. 17, 1459–1471.

Wang, M., Hoogendoorn, S.P., Daamen, W., van Arem, B., Happee, R., 2015. Game theoretic approach for predictive lane-changing and car-following control. Transport. Res. Part C: Emerg. Technol. 58, 73–92.

Wang, X., Jiang, R., Li, L., Lin, Y., Zheng, X., Wang, F.-Y., 2018. Capturing car-following behaviors by deep learning. IEEE Trans. Intell. Transp. Syst. 19, 910–920.

Wu, N., 2002. A new approach for modeling of fundamental diagrams. Transport. Res. A – Pol. Pract. 36, 867–884.

Xiao, L., Wang, M., Schakel, W.J., Shladover, S.E., van Arem, B., 2016. Modeling Lane Change Behavior on A Highway With a High Occupancy Vehicle Lane with Continuous Access and Egress. Transportation Research Board, Washington, D.C.

Xiao, L., Wang, M., van Arem, B., 2017. Realistic car-following models for microscopic simulation of adaptive and cooperative adaptive cruise control vehicles. Transport. Res. Rec.: J. Transport. Res. Board 2623, 1–9.

Yuan, K., Knoop, V.L., Hoogendoorn, S.P., 2015. Capacity drop relationship between speed in congestion and the queue discharge rate. Transp. Res. Rec. 72–80.

Yuan, K., Knoop, V.L., Hoogendoorn, S.P., 2017. A microscopic investigation into the capacity drop: impacts of longitudinal behavior on the queue discharge rate. Transport. Sci. 51, 852–862.

Zhao, L., Sun, J., 2013. Simulation framework for vehicle platooning and car-following behaviors under connected-vehicle environment. In: Intelligent and Integrated Sustainable Multimodal Transportation Systems Proceedings from the 13th Cota International Conference of Transportation Professionals (Cictp2013), 96, 914–924.

Zhou, M., Qu, X., Li, X., 2017. A recurrent neural network based microscopic car following model to predict traffic oscillation. Transport. Res. C: Emerg. Technol. 84, 245–264.